Science of the Total Environment 818 (2022) 151736

Contents lists available at ScienceDirect

Science of the Total Environment

journal homepage: www.elsevier.com/locate/scitotenv

The ballast effect controls the settling of autochthonous organic carbon in three subtropical karst reservoirs

Yu Wei [a], Hao Yan [b,a,*], Zaihua Liu [a,c], Cuihong Han [a], Song Ma [a], Hailong Sun [a], Qian Bao [a]

[a] State Key Laboratory of Environmental Geochemistry, Institute of Geochemistry, CAS, Guiyang 550081, Guizhou, China
[b] International Center for Isotope Effects Research, School of Earth Sciences and Engineering, Nanjing University, Nanjing 210023, China
[c] CAS Center for Excellence in Quaternary Science and Global Change, 710061 Xi'an, China

HIGHLIGHTS

- We find that 30–60% of the settled organic carbon (OC) is autochthonous OC (AOC).
- The reservoir with highest eutrophic state has the lowest settling flux of AOC.
- Biogenic Si and lithogenic minerals enhance AOC settling flux in reservoirs.

GRAPHICAL ABSTRACT

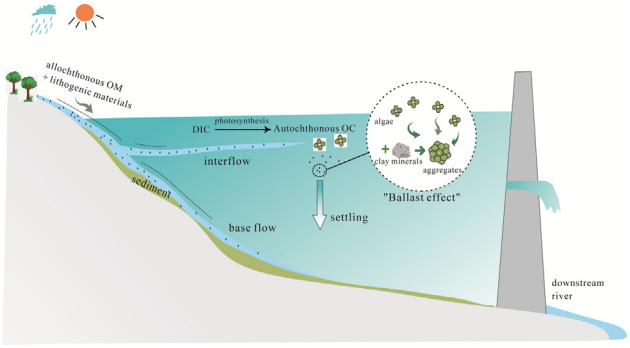

ARTICLE INFO

Article history:
Received 6 August 2021
Received in revised form 12 November 2021
Accepted 13 November 2021
Available online 26 November 2021

Editor: Ashantha Goonetilleke

Keywords:
Autochthonous organic carbon
Reservoir
Ballast effect
Settling flux
Stable carbon isotopes
C/N ratio

ABSTRACT

The change in hydrodynamics by damming facilitates the terrestrial biological-carbon-pump (BCP) effect and promotes the generation and burial of autochthonous organic carbon (OC_{auto}). To constrain the burial fluxes of OC_{auto} is crucial when assessing the role of inland waters in the global carbon cycle as OC_{auto} originating mainly from weathering-derived dissolved inorganic carbon is overlooked in current global carbon budgeting. Here we examined the elemental and carbon isotopic compositions of the settling organic matter collected by sediment traps in three subtropical karst reservoirs (Hongfenghu, Pingzhai and Puding), SW China. The results show that 30– 60% of the settling OC in the studied reservoirs is autochthonous. The proportion of OC_{auto} correlates inversely with OC's settling flux. Interestingly, Hongfenghu Reservoir, featured by the highest trophic state and POC concentration, has the highest fraction of OC_{auto} but the lowest settling flux of OC_{auto} among three reservoirs. The ballast effect of biogenic silica and lithogenic materials, rather than the aquatic primary productivity, is supposed to be the primary factor that governs the settling flux of OC_{auto} in the studied reservoirs. Finally, it is estimated that the settling flux of OC_{auto} in the three reservoirs is 47– 119 g C/m^2/yr while the burial flux of OC_{auto} is 10– 26 g C/m^2/yr if assuming about 80% of OC_{auto} is remineralized after sedimentation. This study demonstrates for the first time the role of biogenic silica and lithogenic materials' input in reservoir OC's settling which may be the further important due to the strengthening agricultural activity and the increasing fast-flow hydroelectric reservoirs.

* Corresponding author at: International Center for Isotope Effects Research, School of Earth Sciences and Engineering, Nanjing University, Nanjing 210023, China.
E-mail address: yanhao@nju.edu.cn (H. Yan).

http://dx.doi.org/10.1016/j.scitotenv.2021.151736

1. Introduction

As global carbon cycle is one of the crucial factors that regulate climate change, carbon transformation and accumulation among different carbon reservoirs are widely concerned. Terrestrial carbon reservoirs (e.g., forest, soil, lakes and reservoirs) are quite active, thus playing an essential role in the global carbon cycle (Beerling and Woodward, 2001; Cole et al., 2007; Marwick et al., 2015; Raymond, 2005; Raymond et al., 2013; Schimel et al., 2015; Sitch et al., 2008; Smith et al., 1993). After the landmark paper of Cole et al. (2007), a new concept of an "active pipe", contrast to the traditional view on inland waters as a "passive pipe" transporting carbon from land to sea, has been accepted in the community. Inland waters can lose carbon not only by evasion to the atmosphere but also by retention in the sediments. Although previous studies have shown that inland water bodies (including reservoirs and lakes) have a similar, perhaps even larger, organic carbon (OC) burial flux compared with oceans (Dean and Gorham, 1998; Mendonça et al., 2017), less attention has been paid to C burial than CO_2 and CH_4 emission from inland waters in past decades (Tranvik et al., 2018). Among the main inland water bodies, reservoirs constitute up to 40– 50% of organic carbon burial flux in inland waters annually (Dean and Gorham, 1998; Mendonça et al., 2017; Mulholland and Elwood, 1982). High mass sedimentation rate in reservoirs also reduces organic carbon oxidation and thus increases organic carbon burial efficiency (Mendonça et al., 2016, 2017; Sobek et al., 2009), making reservoirs a significant carbon sink on a long-term scale (Mulholland and Elwood, 1982; Shi et al., 2018; Tranvik et al., 2009).

Generally, the organic carbon buried in reservoir sediments can be divided into allochthonous OC and autochthonous OC. Autochthonous OC (OC_{auto}) is generated by in-reservoir primary production, while allochthonous OC (OC_{allo}) comes from land. Since a large fraction of carbon utilized by aquatic photosynthesis is derived from rock weathering, some researchers suggest that OC_{auto} buried in inland waters represents an important yet unaccounted carbon sink in the present models of the global carbon cycle (Liu et al., 2017, 2018). Thus, it is necessary to identify the OC sources and settling rate of OC_{auto} when assessing the role of reservoirs in terrestrial carbon cycle.

The sources of OC in rivers, lakes and reservoirs have been investigated by a number of studies for decades (Kunz et al., 2011; Mendonça et al., 2016; Mulholland and Elwood, 1982; Huang et al., 2020; Zheng et al., 2020). Traditional view suggested that rivers, lakes and reservoirs are recipients of organic matter from the watershed and the delivered OC are from terrestrial input. Considering the conditions of illumination and nutrition could be greatly improved after rivers blocked by dams, it is rational that OC generated by aquatic photosynthesis will account for a certain portion of OC retained in reservoir (Jiang and Ji, 2013; Kunz et al., 2011; Maavara et al., 2017; Mendonça et al., 2016; Zheng et al., 2020). However, the relative proportion of OC_{auto} in reservoir sediments varies greatly, from ~0% to >80% at local and regional scales according to previous studies (Jiang and Ji, 2013; Mendonça et al., 2016; Yang et al., 2017; Zheng et al., 2020). To understand the cause of large variabilities in the proportion and flux of OC_{auto} in reservoir sediments is crucial to budget the carbon source and sink in reservoirs at the watershed scale.

The interaction between minerals and organic matter has been found to play a crucial in the present carbon cycle and geological time scale (Caves Rugenstein et al., 2019; Cotrufo et al., 2019; Galy et al., 2007; Kennedy et al., 2002). A large fraction of OC in oceans is settled in association with inorganic minerals (i.e., calcite, opal, and clay) as mineral phases may enhance the settling of organic matter by increasing the density and sinking speeds of particle aggregates (the so-called "ballast effect") (Armstrong et al., 2001; Blattmann et al., 2019; Honda and Watanabe, 2010; Klaas and Archer, 2002; Rixen et al., 2019; Passow and De La Rocha, 2006). This is evidenced by the strong correlations observed in the deep ocean between the vertical fluxes of particulate organic carbon (POC) and of inorganic materials (calcite, opal, and clay) (Klaas and Archer, 2002). Similarly, OC in rivers can be transported with mineral particles and then deposited in reservoirs, lakes, or at the estuary, continental shelf (Galy et al., 2007; Hage et al., 2020; Tao et al., 2015). While the ballast effect of clay, calcite and opal in marine environment is well known, its role in inland water bodies is unrevealed despite having a higher transportation capability of clay minerals than oceans.

Governments worldwide mitigated the shortage of water resources and developed hydropower by building thousands of reservoirs, including in the karst areas. It is known that surface water in karst catchments has higher concentrations of dissolved inorganic carbon (DIC) than in non-karst catchments. Previous studies have suggested that high HCO_3^- concentration can promote not only calcite precipitation but also the primary productivity of hydrophytes and phytoplankton (Yang et al., 2016; Zeng et al., 2019). In addition, recent study showed that, due to high aquatic primary productivity and high pH value in the epilimnion, karst freshwater reservoirs can have a negative evasion flux of CO_2 from water to atmosphere seasonally, which is apparently different from the observation in non-karst reservoirs (Pu et al., 2020). Therefore, in this study, we selected three subtropical karst reservoirs in Guizhou Province (SW China) with similar land use in the catchments but different hydrodynamics and algal communities. Stable carbon isotope composition ($\delta^{13}C$) and C/N ratios were used to track the sources of the settling OC collected by sediment traps. The aim of our study is to determine the settling flux of OC_{auto} in karst reservoirs and explore the role of algal community and input of lithogenic materials in the settling of OC_{auto}.

2. Materials and methods

2.1. Site description

Three reservoirs, Pingzhai Reservoir (PZR) and Puding Reservoir (PDR) in the Sancha River Basin as well as Hongfenghu Reservoir (HFR) in the Maotiao River Basin, were selected as our study sites (Fig. 1).

With an area of 4860 km^2 in northwestern Guizhou Province (SW China), the Sancha River Basin is a typical karst peak cluster-depression basin. The Sancha River, 325.6 km in length, is a primary tributary of the Wujiang River. The bedrock underlying the study area consists mainly of carbonate rocks and a small amount of sandstone and shale. There is a well-developed belowground river network in the Sancha River Basin. Most of the karst landform develops vertically, resulting in large areas of steep slopes (Cai et al., 2015) and favorable conditions for soil erosion. The study area's soil layers are thin with a low formation rate, and a lack of a semi-weathered parent material layer. Weak adhesion between the soils and rocks makes this region prone to soil erosion and sliding of soil blocks (Cai et al., 2015). The Sancha River Basin has a subtropical monsoon climate with abundant precipitation (annual average of approx. 1100 mm), most of which falls between May and October. The study area is densely populated. The local karst topography has a fragmented surface with scattered farmland on it. Poorly managed land use has resulted in severe soil erosion (Wang et al., 2019). There are more than twenty reservoirs in the Sancha Basin, of which Pingzhai Reservoir (PZR) and Puding Reservoir (PDR) are the largest ones. Both PZR and PDR are river-valley reservoirs. As a newly built reservoir in 2015, PZR has experienced little pollution and remains an Oligo-Meosotrophic water body. In comparison, PDR, adjoining with populated regions, has a relatively high trophic state.

The Maotiao River Basin is located in the central part of Guizhou Province and covers 3109 km^2 (Fig. 1). The annual average temperature in the basin is 14.2 °C, and the average annual precipitation is 1300 mm, most of which occurs between May and September. Permian-Triassic limestone covers more than 80% of the watershed, and karst landforms in the watershed develop well. Agriculture is the primary human activity in this area, and the major crops are rape, rice, bean and maize. Land covers in the watershed have experienced remarkable changes due to the rapid development in the economy over recent years. Hongfenghu Reservoir (HFH), built in 1960, is the Maotiao River Basin's first reservoir. Years of human activities have resulted in severe eutrophication at HFH. In contrast to PZR and PDR, HFH is a lake-type reservoir with weak hydrodynamics, evidenced by the longer residence time (Table 1) and lower flow velocity (Li

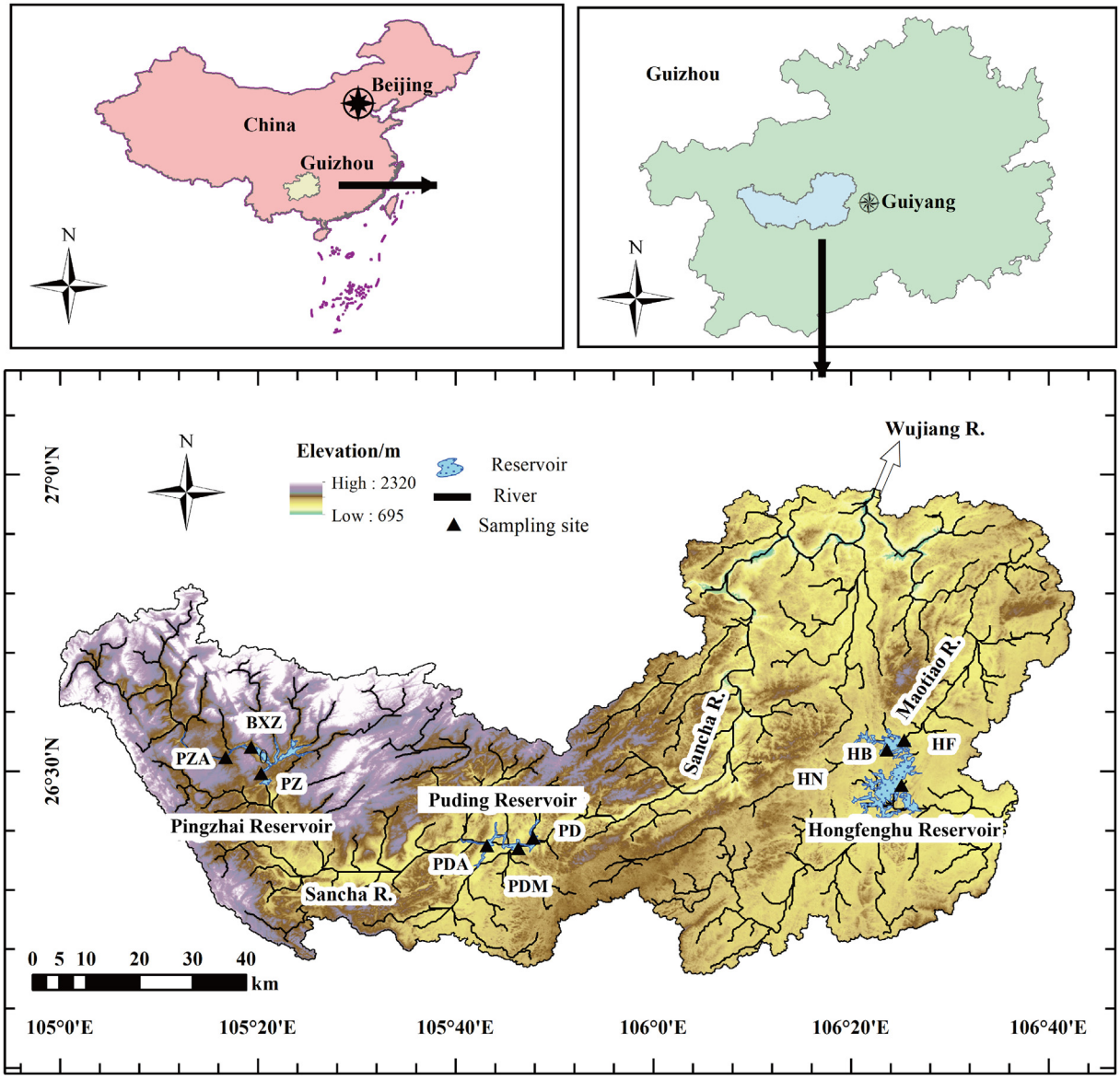

Fig. 1. Locations of the studied reservoirs, sediment trap deployment and water sample collecting sites.

et al., 2019). All of three reservoirs are deep-water reservoirs, which exhibit seasonal thermal stratification during the period from late spring to early autumn. The general characteristics of three reservoirs are given in Table 1.

2.2. Sampling and analysis

Three sites were selected at each reservoir (Fig. 1; PZA, BXZ and PZ in PZR; PDA, PDM and PD in PDR; HN, HB and HF in HFH) for hydrochemical monitoring and water sampling vertically and to place the sediment traps. Five filed campaigns (two-month interval) were conducted to do the on-site hydrochemical monitoring and sample collection from Mar. 31, 2018 to Jan. 15, 2019 throughout a hydrological year. Water temperature (WT), pH, electrical conductivity (EC), dissolved oxygen (DO), and turbidity were measured from the surface to the bottom of the water column using multi-parameter water quality meters (WTW 350i and YSI EXO 3), which were pre-calibrated using standards for pH (4 and 10), EC and DO (100%). The accuracies for WT, pH, EC, DO, and turbidity were 0.01 °C, 0.05, 0.1 μS/cm, 0.01 mg/L, and 0.01 FNU, respectively. 0.8– 1.2 L water was taken at different depths (0– 0.5 m,10 m, 20 m, 40 m, 80 m, and 120 m, depending on water depth). The samples were then filtrated through a 0.7 μm glass filter (Whattman GF/F, pre-combusted at 450 °C for 4 h), washed with 5 mol/L HCl and stored at 4 °C for further analysis. Sediment traps (cylindrical, length = 1.4 m, diameter = 14 cm) were deployed at 10 m, 20 m, 30 m, 40 m, and 80 m depth (depending on the

Table 1
General information of Hongfenghu Reservoir, Puding Reservoir and Pingzhai Reservoir.

	Water area /km^2	Watershed area/km^2	Volume/m^3	Maximum depth/m	Retention time /days	Trophic state	Dominant phytoplankton
Pingzhai Reservoir	21.70	3492	10.9×10^8	120	80.4	Oligo-Mesotrophic	Diatom
Puding Reservoir	10.95	5871	4.2×10^8	50	40.6	Meoso-Eutrotrophic	Diatom
Hongfenghu Reservoir	42.91	1596	7.5×10^8	40	119	Eutrophic	Cyanobacteria, diatom

Notes: Water retention times are from Xiang et al. (2016), while phytoplankton community and trophic state data are from Xiao et al. (2019).

water depth) and retrieved every two months. Settling particulates collected by sediment traps were freeze-dried in the lab, then weighted and crushed to 200 mesh for further analysis. Eleven surface soil samples (<10 cm) were collected in the catchment and pretreated in the same way as the sediment trap samples.

All laboratory work, including SEM observations, elemental analyses, and stable isotope measurements, was conducted at the Institute of Geochemistry, Chinese Academy of Sciences (IGCAS). Carbon (TOC/TC) and nitrogen (TN) concentrations were measured by vario MACRO cube elemental analyzer, with relative precision <2%. TIC was determined as the difference of TC and TOC (TIC = TC-TOC) and the calcium carbonate ($CaCO_3$) contents were calculated as 100/12 × TIC (100 and 12 are the molar weights of $CaCO_3$ and C respectively). C/N ratios of organisms were reported in atom ratio. Carbon isotopic analyses were performed in a continuous-flow mode using a MAT 253 isotope ratio mass spectrometry (IRMS) equipped with vario MACRO cube elemental analyzer for combustion. The results are reported relative to Vienna Pee Dee Belemnite (VPDB). The reproducibility of isotopic measurements is ~0.1‰ based on repeated measurements of laboratory standards. The samples for the analysis of TOC, C/N and carbon isotope composition of OC were pre-treated with 5 N HCl to remove carbonate minerals. Then the residues were rinsed with ultrapure water and freeze-dried. Six samples collected in summer at 0– 0.5 m depth (suspended particles) and the bottom (sediment trap samples) near the dam of each reservoir, i.e., PZ, PD and HF, were selected for scanning electron microscope (SEM) observation which was conducted with FEI Scios dual-beam focused ion beam/scanning electron microscope (FIB/SEM) system. And three suspended particle samples at the depth of 10 m at the dam site of each reservoir were collected in August for particle size distribution analysis with Mastersizer 2000 Laser Particle Size Analyzer. The exact sampling locations, dates and data of suspended particles, trapped materials, soils and hydrochemistry parameters were listed in Tables S1 and S2. Besides, the biogenic Si concentrations of settling particles, Chl-a concentrations used in this study were compiled from Wei et al. (2020) and Han et al. (2020), respectively, and listed in Tables S1 and S2.

2.3. Calculation and analysis methods

The settling flux of particles (F_{total}) and organic carbon (F_{OC}) were calculated as following:

$$F_{\text{total}} = \frac{M}{A \times T} \tag{1}$$

$$F_{\text{OC}} = F_{\text{total}} \times OC(\%) \tag{2}$$

where M (g) donates the total mass of settling particles collected by sediment traps during the deployment period T (days), and A donates the surface area (m^2) of sediment traps which is 0.012 m^2 for our sediment traps.

A binary mixing model was employed to quantify the contributions of OC_{allo} and OC_{auto} to the settling OC. Based on mass balance, one gets (Perdue and Koprivnjak, 2007)

$$\frac{X_{\text{OC-auto}}}{X_{\text{OC-allo}}} = \frac{C/N_{\text{auto}}}{C/N_{\text{allo}}} \times \frac{C/N_s - C/N_{\text{allo}}}{C/N_{\text{auto}} - C/N_s} \tag{3}$$

$$X_{\text{OC-auto}} + X_{\text{OC-allo}} = 1 \tag{4}$$

where C/N_{auto}, C/N_{allo}, and C/N_s donate the C/N values of autochthonous endmember, allochthonous endmember, and sediment samples, respectively. To account for the uncertainty in endmember values, we did Monte Carlo simulation to calculate $X_{OC\text{-}auto}$ and its errors. 1 × 10^6 runs were performed to generate the possible C/N ratios with random endmember values within each range and variable $X_{OC\text{-}auto}$ values (from 0 to 1 with an increment of 0.01). Then the generated C/N ratios were compared with those of settling samples. An effective estimation of $X_{OC\text{-}auto}$ was obtained when the generated C/N ratio deviated from the measured one by <0.01. To attain the stability of the model, the above process was repeated by 1 × 10^3 times for each sample. Finally, the mean value and the standard deviation of all the possible $X_{OC\text{-}auto}$ were adopted as the final $X_{OC\text{-}auto}$ value and the error bar for each sample. The simulation was run on MATLAB R2016a.

In this study, primary productivity (PP) was estimated using the following equation (Wang et al., 2011):

$$\text{PP} = (3.7 \times \text{Chl-a} \times E \times D)/2 \tag{5}$$

where Chl-a is the concentration of chlorophyll *a* and has been reported by Han et al. (2020); D is the length of daytime and set to be 12 h; E donates euphotic depth which was measured on-site as 3 times of Secchi disc depth (m).

3. Results

3.1. Physic-chemical properties of reservoir water

The three reservoirs displayed clear seasonal and vertical variations in water temperature, pH, EC, and DO. Water temperature (WT) varied from 6.86 °C to 29.07 °C, and the average WT was 16.94 ± 5.00 °C. Besides, WT decreased from HFH (6.86– 29.07 °C, average = 17.54 ± 6.44 °C), PDR (9.17– 27.53 °C, average = 17.15 ± 4.73 °C) to PZR (10.54– 26.40 °C, average = 16.40 ± 4.04 °C), which is related to the attitude of each reservoir. pH varied from 7.25 to 9.18, and the average pH value was 7.94 ± 0.45 °C. No systematic trend in pH was observed among HFH (7.25– 8.96, average = 7.89 ± 0.53), PDR (7.45– 8.90, average = 8.03 ± 0.35) and PZR (7.35– 9.18, average = 7.91 ± 0.46). EC varied from 247.4 μS/cm to 487.00 μS/cm with the average of 389.71 ± 42.86 μS/cm. EC in HFH (247.40– 487.00, average = 362.33 ± 42.70) was lower than those in PDR (315.80– 455.10, average = 407.45 ± 29.18) and PZR (250.80– 454.30, average = 394.78 ± 43.10). The concentrations and saturation of DO were 7.73 ± 3.05 mg/L (0.08– 14.50 mg/L) and 89.37 ± 38.16% (1.1– 202.4%), respectively, with the lowest values observed in HFH (6.17 ± 4.03 mg/L and 70.31 ± 45.97%). PDR had the highest concentrations and saturation of DO which were 8.89 ± 1.91 mg/L (6.17– 13.91 mg/L) and 109.48 ± 25.44% (81.1– 201.10%) respectively.

Thermal and chemical stratification existed in all three reservoirs from March to August (Fig. S1). Results of in-situ physicochemical measurements in January and June are plotted in Fig. 2 to show the different properties during mixing and stratification periods. During the stratification period, the depth of epilimnion was about 5 m. Within the epilimnion layer, water temperature, pH, DO, and turbidity were higher but EC was lower than in the hypolimnion (Fig. 2). Because Ca^{2+} and HCO_3^- were the dominant ions in karst waters, low EC in the epilimnion indicated the depletion of Ca^{2+} and HCO_3^- in the surface layer of the water column. During the stratification period, DO in the epilimnion was highly supersaturated (>100%) in three reservoirs. DO decreased rapidly at a depth of 5– 10 m, especially in HFH, where DO_{sat} was less than 20% in the hypolimnion (Fig. 2). Different patterns of EC in the hypolimnion were observed among three reservoirs. EC decreased slightly with increasing depth in PDR while it increased significantly with depth in HFH. In PZR, EC showed no variation with depth except a trough of low EC at a depth of ~20 m, corresponding to a higher turbidity at this depth, indicating the presence of interflow. During the mixing period, all parameters were almost vertically uniform (Fig. 2). An anomaly is a rapid increase in EC and turbidity at the bottom of the water in HFH. PDR had the highest turbidity during the study period, consistent with its strongest hydrodynamics of three reservoirs.

The primary productivity (PP) varied from 0.28 to 1.08 g/m^2/d with the average of 0.68 ± 0.24 g/m^2/d. PP was the highest in in PZR (0.82 ± 0.26 g/m^2/d), followed by HFH (0.69 ± 0.14 g/m^2/d) and PDR (0.40 ± 0.13 g/m^2/d).

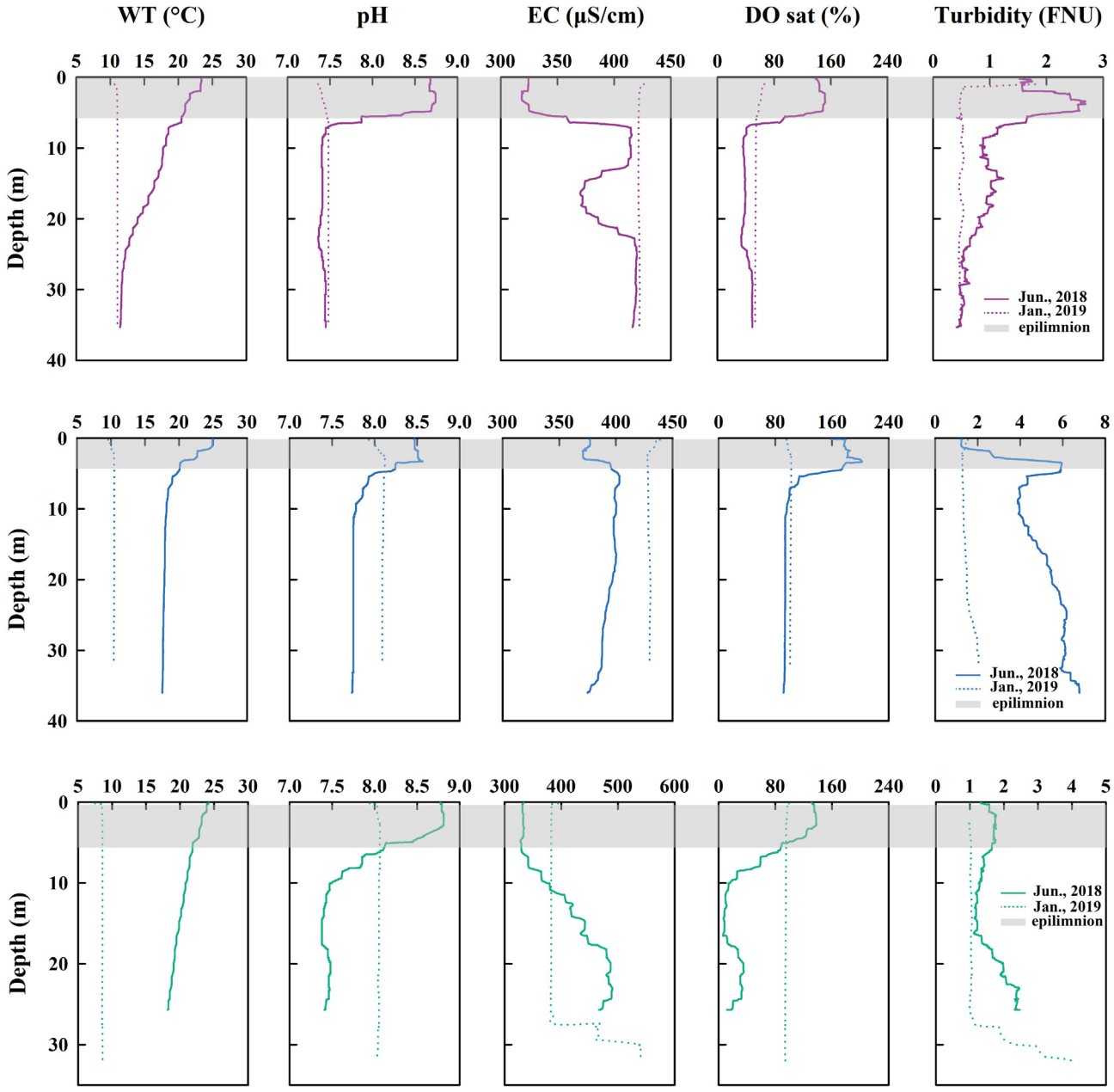

Fig. 2. Vertical profiles of water temperature (WT), pH, specific electronic conductivity (EC), dissolved oxygen saturation index (DO_{sat}) and turbidity. The upper, middle, and lower panels denote the results measured at the sites in front of each dam in the Pingzhai Reservoir, Puding Reservoir, and the Hongfenghu Reservoir. The solid lines represent the data in June 2018, while the dashed lines are for the data in January 2019.

3.2. Geochemical properties and their variations of suspend particles

The concentrations of suspended particulate organic carbon (POC) in the three reservoirs varied from 0.02 to 4.50 mg C/L, with an average of 0.70 ± 0.81 (1SD) mg C/L. Generally, averaged POC concentration was higher during the stratification period than during the mixing period, i.e., 1.04 ± 0.88 mg C/L vs. 0.16 ± 0.07 mg C/L. POC concentration was much higher in the epilimnion than in the hypolimnion during the stratification period, while it exhibited no vertical variation during the mixing period in all three reservoirs (Fig. 3a). $\delta^{13}C$ of POC ($\delta^{13}C_{POC}$) showed a range from −36.0 to −18.7‰, with an average value of −29.6 ± 3.4‰. Similar to POC concentration, $\delta^{13}C_{POC}$ values were higher during the stratification period. No clear trend in $\delta^{13}C_{POC}$ values was observed vertically (Fig. 3b). The C/N ratio of suspended particulate organic matter ranged from 2 to 14, which was slightly lower during the mixing period than during the stratification period (Fig. 3c).

Based on SEM observations, the suspended particles in the surface layer were mainly composed of diatom cells, calcite crystals and biofilm which may be the residues of cyanobacteria (Fig. 4a, b, and c). Noteworthily, abundant diatom cells were observed in PZR and PDR (Fig. 4a and b), while biofilm was abundant in HFH (Fig. 4c). This observation is in consistent with the phytoplankton community structure of the studied reservoirs (Table 1). The size of suspended particle varied among three reservoirs (Fig. S2). The suspended particles in HFH had the smallest sizes (27.54 ± 23.46 μm), followed by PZR (72.75 ± 102.30 μm) and PDR (93.06 ± 93.79 μm).

3.3. Geochemical properties and fluxes of settling particles

Fig. 3d shows the fluxes of settling particles (F_{total}) in three reservoirs based on the amounts of trapped materials. F_{total} varied largely among the three reservoirs, from 0.26 to 54.83 g/m^2/d. It is seen that PDR had the

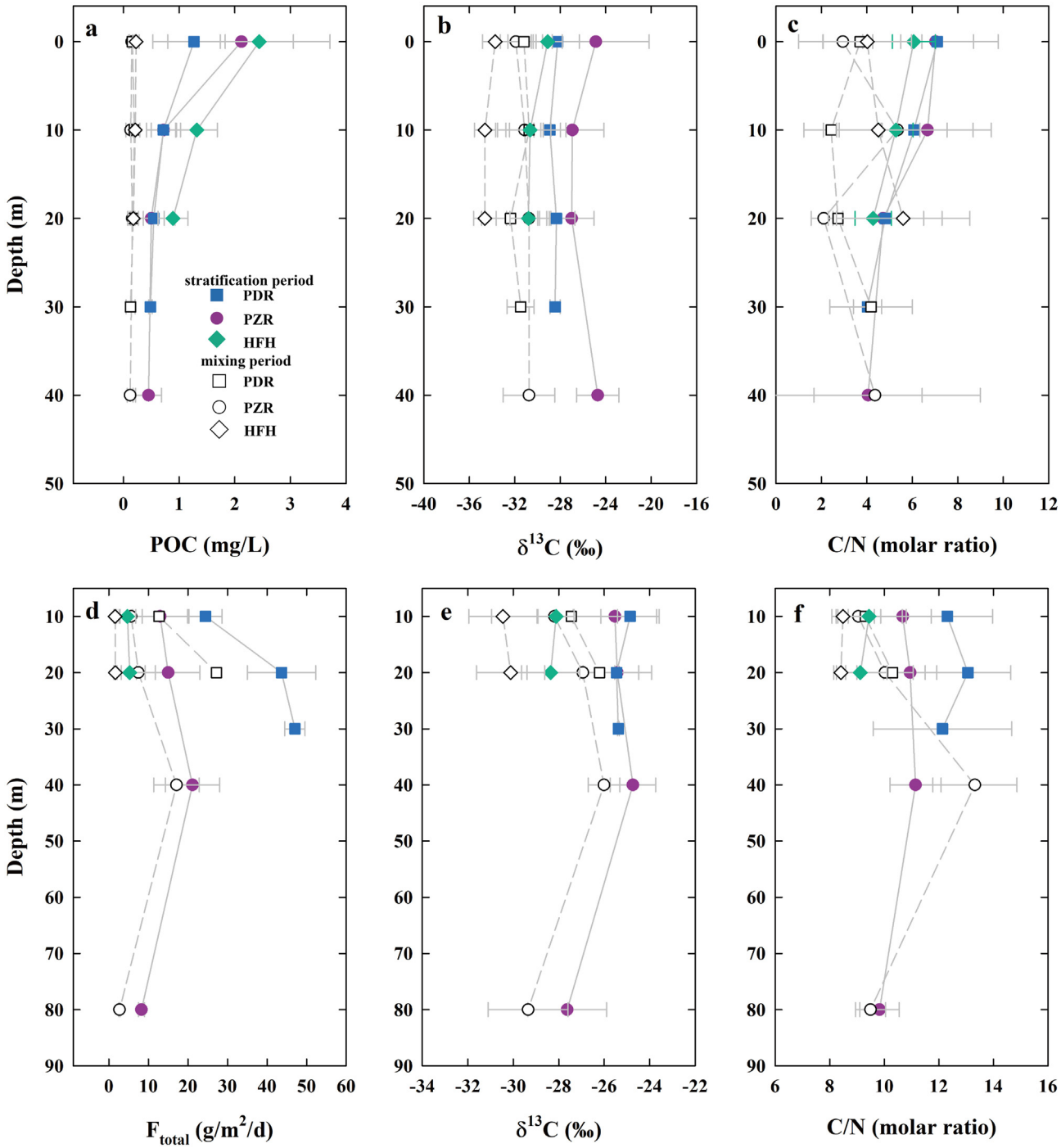

Fig. 3. Vertical profiles of concentrations of POC (a), carbon isotope composition ($\delta^{13}C$) of POC (b), atomic C/N ratios of suspended particulate organism (c), as well as the fluxes of sinking particles (d), the $\delta^{13}C_{OC}$ in sinking particles (e) and atomic C/N ratios of organism in sinking particles (f). Solid and hollow symbols denote the stratification and mixing periods, respectively. The circles, rectangles and diamonds represent the Pingzhai Reservoir (PZR), Puding Reservoir (PDR) and Hongfenghu Reservoir (HFH), respectively.

highest F_{total}, followed by PZR and HFH. F_{total} showed an increase with depth in PDR but no vertical variation in HFH. In PZR, F_{total} reached the maximum value at a depth of 40 m. For all three reservoirs, F_{total} was higher during the stratification period. In contrast, stable isotope composition of organic carbon ($\delta^{13}C_{OC}$) and C/N ratios of settling particles showed no obverse vertical trend. Seasonally, $\delta^{13}C_{OC}$ and C/N ratios of settling particles were also higher during the stratification period than during the mixing period (Fig. 3e and f).

Organic carbon (OC) in settling particles in three reservoirs accounted for 2.62– 12.99% of the total settling mass. HFH has the highest contents of OC, followed by PZR and PDR. An exponentially inverse correlation between OC's content in settling particles and F_{total} was observed in three reservoirs (Fig. 5a). The increasing trend in F_{total} coupled with the decreasing trend in the content of OC reflects the growing input of terrestrial materials from HFH to PDR, evidenced by the relationship between $\delta^{13}C_{OC}$ of settling particles and F_{total} (Fig. 5b). The settling particles having the lowest settling flux and the highest OC proportion in HFH was featured by relatively low $\delta^{13}C_{OC}$ values among the three reservoirs. As the F_{total} increased, the $\delta^{13}C_{OC}$ value of settling particles increased and reached a plateau at the value of ca. −25‰, which reflects the $\delta^{13}C_{OC}$ values of soil endmember

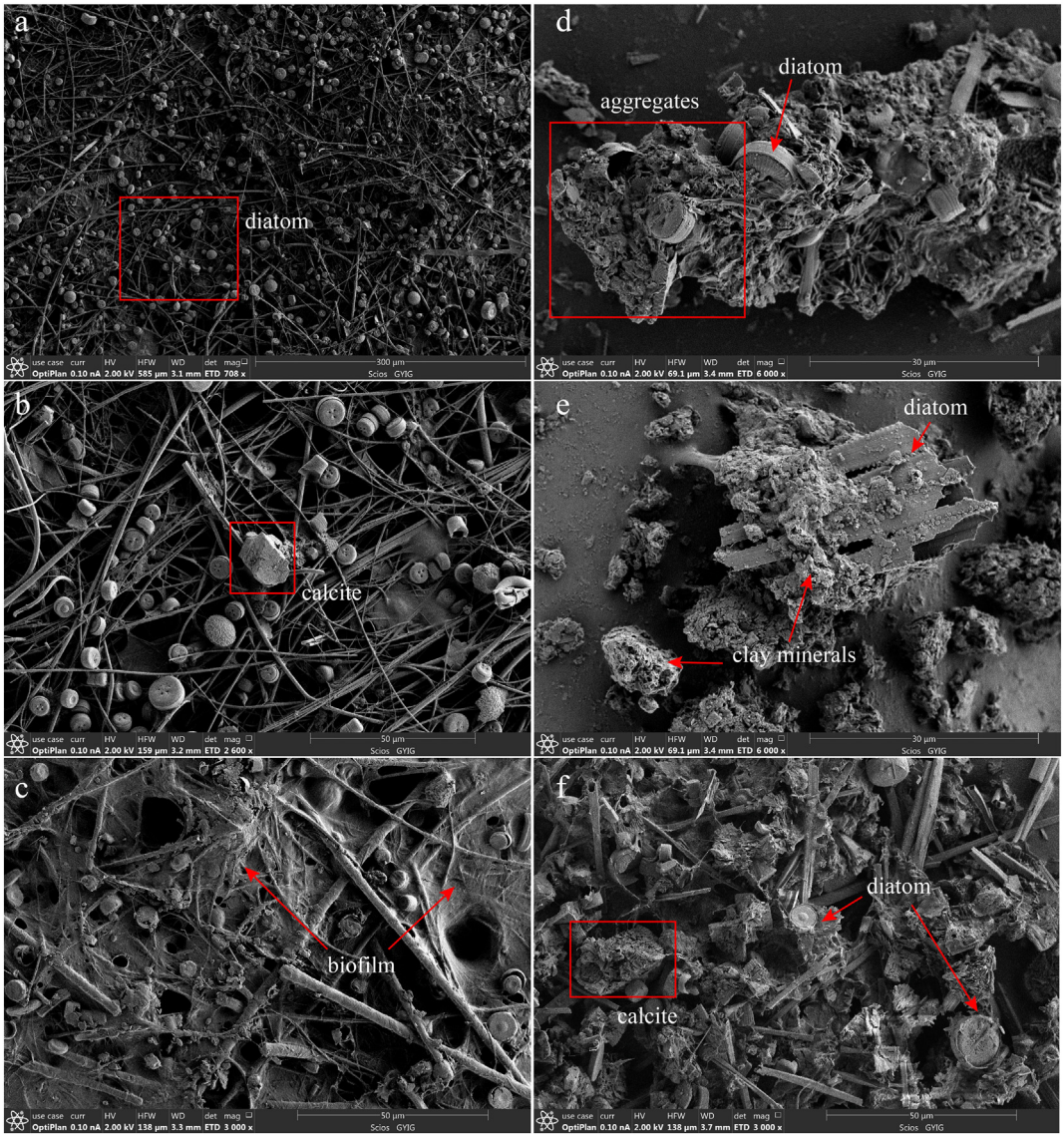

Fig. 4. Scanning electronic microscopic (SEM) images for suspended (a-c) and settling particles (d-f). Suspended particles in (a), (b) and (c) were collected in the surface water layer at sites PZ, PD, and HF, respectively. Samples in (d) was collected at PZ at 80 m depth, in (e) collected at PD at 30 m depth, and in (f) collected at HF at 20 m depth.

in the catchment ($-25.3 \pm 1.3‰$). The coincidence of $\delta^{13}C_{OC}$ values in PDR with soil endmember implies a dominant contribution of allochthonous OC in the sediments.

Similar to suspended particles, distinct compositions of settling particles were observed among reservoirs. Based on SEM observations, the settling particles were mainly composed of diatom, calcite crystals and lithogenic minerals (Fig. 4d, e and f). Abundant lithogenic minerals were present in the settling particles in PZR and PDR (Fig. 4d and e), but absent in HFH (Fig. 4f). Further X-Ray Diffraction (XRD) experiments showed that lithogenic materials mainly consisted of quartz, Fe/Mn oxides, and clay minerals.

4. Discussion

4.1. Sources of organic carbon in settling particles

More than 16 million dams are over the world, and the number is still increasing rapidly (Lehner et al., 2011; Maavara et al., 2017). The massive building of dams has significantly altered the riverine transport of OC and nutrients (Maavara et al., 2015, 2020). Due to the high sedimentation rate and burial efficiency, increasing attention has been paid to the role of artificial reservoirs as a carbon sink in the terrestrial carbon cycle (e.g., Mendonça et al., 2012, 2014, 2017). However, it is imperative to constrain the fraction of OC_{auto} in reservoir sediments, because burial of OC_{auto} can only be regarded as an additional carbon sink after damming (Liu and Dreybrodt, 2015; Liu et al., 2018; Mendonça et al., 2017).

In previous studies (e.g., Meyers, 1994; Tao et al., 2009; Maki et al., 2010; Rodríguez-Murillo and Filella, 2015; Zheng et al., 2020), either C/N ratios or $\delta^{13}C$ is commonly used to determine OC sources in inland waters. It is assumed that the top-layer soils collected in the Sancha River Basin and the Maotiao River Basin represent the endmember of allochthonous OC. The average $\delta^{13}C_{OC}$ values of 27 soil samples (11 samples from this study and 16 samples from Liu (2009), see Table S3 for the details) were $-25.3 \pm 1.3‰$ while C/N of them were 14.77 ± 2.84 (Fig. 6). Based on SEM observations, POM collected in the epilimnion layer mainly consisted of phytoplankton and thus was chosen as the endmember of autochthonous OC (Fig. 4a, b and c). Average values of $\delta^{13}C_{OC}$ and C/N ratios of OC_{auto} in three reservoirs were $-29.4 \pm 3.9‰$ and 6.79 ± 2.03 ($n = 26$), respectively (Fig. 6). The $\delta^{13}C_{OC}$ and C/N ratios of OC_{auto} and OC_{allo} endmembers are consistent with the previous studies (e.g., Shi et al., 2018; Meyers and Ishiwatari, 1993). It is shown in Fig. 6 that there was a wild range of $\delta^{13}C$ values of phytoplankton in this study. Various factors,

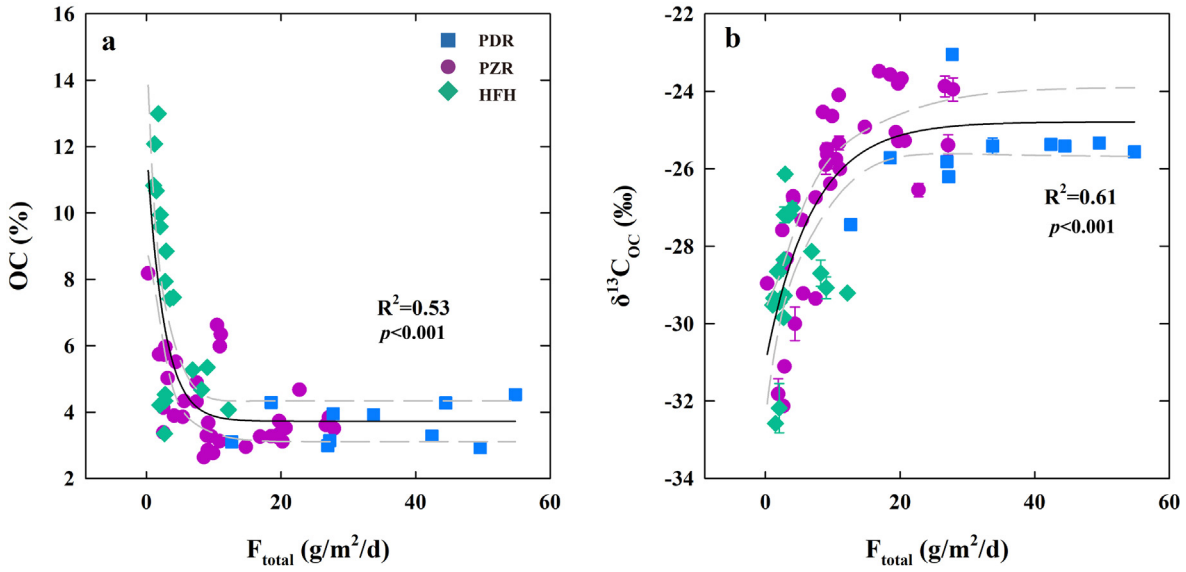

Fig. 5. Scatter plots of settling particle's flux versus the content of OC (a) and the $\delta^{13}C_{OC}$ values in settling particles (b). The circles, rectangles and diamonds represent the Pingzhai Reservoir, Puding Reservoir and Hongfenghu Reservoir, respectively.

including phytoplankton community structure and carbon assimilation mechanism can affect the $\delta^{13}C$ values of phytoplankton. Wang et al. (2013) stated a significant control of phytoplankton community structure on the $\delta^{13}C$ values of phytoplankton in karst reservoirs, SW China. They found the $\delta^{13}C$ values of phytoplankton is lower when Bacillariophyta is dominant, which is contrary to our observation that HFH had the lowest $\delta^{13}C$ values of phytoplankton. We suppose that the large range of $\delta^{13}C_{OC}$ values of OC_{auto} endmember may be caused by the depleting of DIC in epilimnion water and the large carbon isotope fractionation during DIC uptake (Gu et al., 2006; Barth et al., 2017). In this study, the overlap of $\delta^{13}C$ values of two endmembers (see Fig. 6) hindered its application in the source determination. Here, only C/N ratio was used to calculate the fraction of OC_{auto} in the sinking particles ($X_{OC\text{-}auto}$).

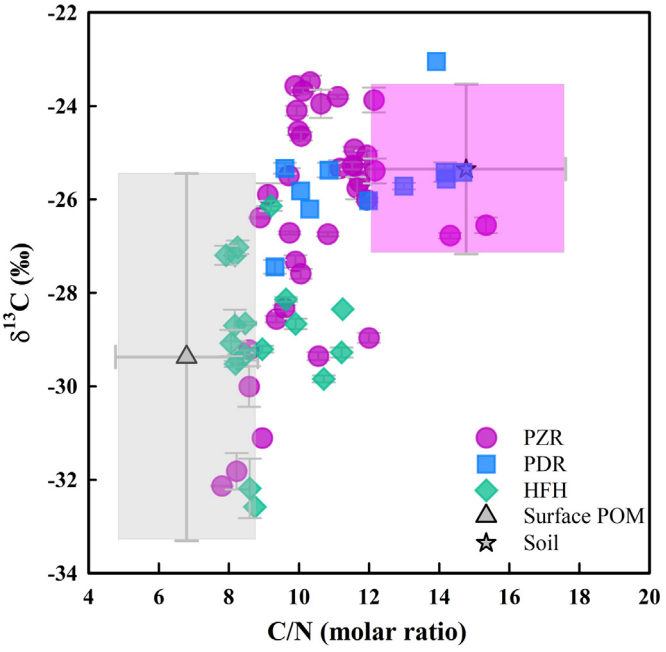

Fig. 6. Scatter plots of carbon isotope compositions and C/N ratios for settling particles, soils and POM in the surface layer.

The results showed that PDR had the lowest proportion of OC_{auto} in settling OC (X_{auto} = 0.30 ± 0.16, 1SD), which is consistent with the fact that PDR had the highest water flow velocity (Li et al., 2019) and the shortest water resistance time, as well as the observation that $\delta^{13}C_{OC}$ of the settling particles in PDR was close to the value of soil endmember (Fig. 5b). As X_{auto} increases, $\delta^{13}C_{OC}$ of the settling particles decreases due to the relatively low $\delta^{13}C_{OC}$ value of OC_{auto} endmember (Fig. 7a). The highest X_{auto} is obtained in HFH where about one-half of settling OC is produced in reservoir (X_{auto} = 0.56 ± 0.11). A significant correlation between X_{auto} and the settling flux of OC (F_{OC}) is observed (Fig. 7b). There is a high F_{OC} when X_{auto} < 0.2, indicating that large import of OC_{allo} is the reason for high F_{OC} in PDR. As X_{auto} increases from 0.11 to 0.4, F_{OC} decreases rapidly and converges to a value of 0.25 ± 0.15 g C/m²/d when X_{auto} > 0.6 (Fig. 7b).

4.2. Controlling mechanism of autochthonous OC settling in the studied reservoirs

When the F_{OC} and X_{auto} are obtained, the settling flux of OC_{auto} ($F_{OC\text{-}auto}$) can be calculated. The highest $F_{OC\text{-}atuto}$ is obtained in PDR (0.32 ± 0.18 g C/m²/d), followed by PZR (0.16 ± 0.08 g C/m²/d) and HFH (0.14 ± 0.08 g C/m²/d). It is noted that organic matter decomposition might take place to our trapped samples. Therefore, the settling flux of OC_{auto} may be underestimated in our study. Goto et al. (2016) found that 57–78% of POC could be retained after 56 days in a fresh water lake with the C/N ratios increasing by 0.5–2. It is difficult to estimate the degradation degree due to the differences in phytoplankton community, temperature, and dissolved oxygen concentration between our study and Goto et al.'s work. Assuming a constant organic flux and daily loss of 0.5% of organism (Gardner et al., 1983) in traps, it showed that ~87% of the settling organism was retained after 60-day deployment. In this case, we suggest that organism decomposition in the traps would not affect our following discussions and conclusions.

Previous studies have found several factors, including primary productivity (PP), degradation, and settling efficiency, can influence the settling flux of autochthonous OC in lakes and reservoirs (e.g., Huang et al., 2020; Meyers and Ishiwatari, 1993; Zheng et al., 2020). Fig. 8a and Fig. S3 show that no correlation exists between PP and $F_{OC\text{-}auto}$. Because the concentration of Chl-a and E in Eq. (5) only represent instantaneous values while $F_{OC\text{-}auto}$ is obtained via sediment trap placed for 2–3 months, the mismatch of sampling time between PP and $F_{OC\text{-}auto}$ may be partly responsible for their uncorrelation. Alternatively, the contents of total organic nitrogen (TON) in the settling particles are used as an indicator of trophic state. As a major nutrient, the supply of nitrogen will promote the growth of

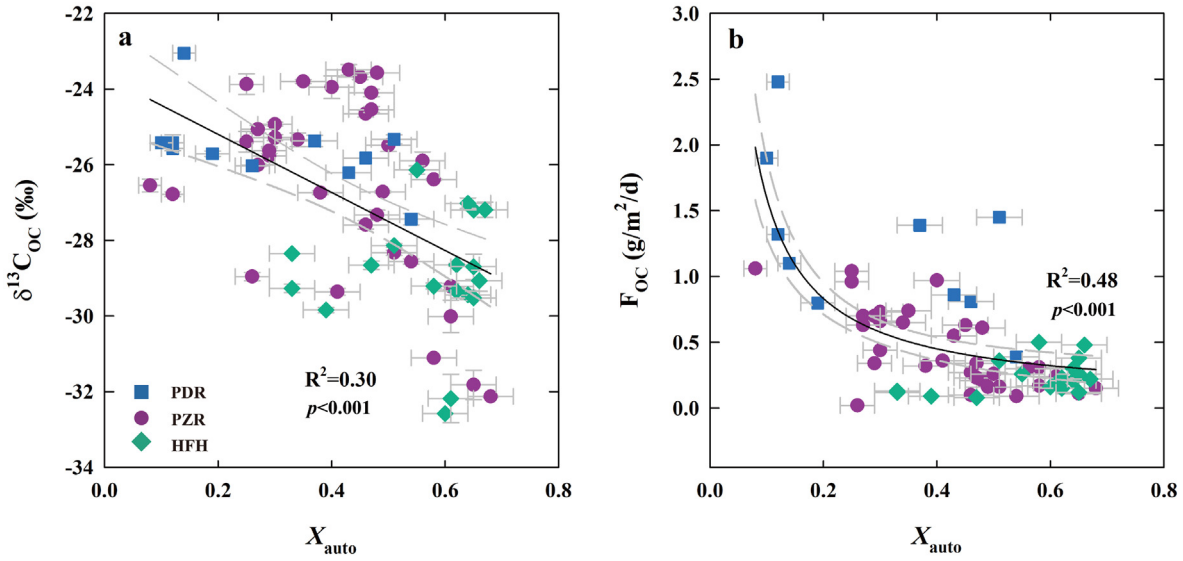

Fig. 7. Scatter plots of the fraction of autochthonous OC versus the $\delta^{13}C_{OC}$ values (a) and the settling fluxes of OC (b). The circles, rectangles and diamonds represent the Pingzhai Reservoir, Puding Reservoir and Hongfenghu Reservoir, respectively.

phytoplankton, resulting in an increase in autochthonous organic carbon burial in lakes (e.g., Heathcote et al., 2015). Thus, it is reasonable that the flux of autochthonous organic carbon in lake sediments is positively correlated with the content of organic nitrogen. However, we observe no correlation between them in this study (Fig. 8b), despite a positive correlation between the contents of TON and TOC ($R^2 = 0.94$, $p < 0.001$) which has also been found in other studies (e.g., Huang et al., 2018; Yu et al., 2018). However, we think such a positive correlation was more likely the result of stoichiometric assimilation of nitrogen and carbon rather than the fertilization effect of nitrogen. Besides, there was no correlation between the contents of biogenic Si and TN ($R^2 = 0.03$, $p = 0.33$), since biogenic Si was mostly from diatom while terrestrial OM contributed a large fraction of TN in sediments. Among the three reservoirs, HFH has the highest trophic state, while PZR and PDR are Oligo-Mesotrophic and Meso-Eutrophic reservoirs respectively. The trophic states of three reservoirs can be well reflected by their different phytoplankton community structures and the abundance of phytoplankton cells. HFH had the highest abundance of phytoplankton cells in epilimnion layer among the three reservoirs. As high as 50% of phytoplankton consisted of Cyanophyta in HFH's surface water, while Cyanophyta was nearly absent in PDR and PZR (Xiao et al., 2019). We do not find that a high OC_{auto} settling flux comes with the high eutrophic level in HFH (Table 2). Therefore, other factors (e.g., hydrodynamic state and phytoplankton community structure), instead of PP and trophic state, may control the settling of OC_{auto} in the studied reservoirs.

There is a weak positive correlation between $F_{OC\text{-}auto}$ and the content of biogenic Si in settling particles (Fig. 8c). Owing to a bigger size (commonly between 20 and 200 μm in diameter or length) and higher density than cyanobacteria, diatoms often have high sinking rates (Honda and Watanabe, 2010). Another reason for the correlation between $F_{OC\text{-}auto}$ and the content of biogenic Si is that, compared to diatom, cyanobacteria is more readily to be degraded before and after deposition (Goto et al., 2016). This explains that diatom was the major component of OC in the SEM images of the settling particles in HFH where biofilm was pervasive in epilimnion layer (Fig. 4c and f).

It is also observed that $F_{OC\text{-}auto}$ correlated positively with the amount of lithogenic materials in traps which were calculated by total mass flux subtracting the mass of calcium carbonate ($CaCO_3$), biogenic opal ($SiO_2{\cdot}0.4H_2O$) (data from Wei et al., 2020), and organic matter (2.2 × OC) (Klaas and Archer, 2002; Rixen et al., 2019). Lithogenic materials (mainly as quartz, Fe/Mn oxides, and clay minerals) account for more than fifty weight percent of the settling particles. Fe/Mn oxides and clay minerals characterized by large specific surface areas have excellent adsorption capacity. Thus, the presence of these minerals can enhance the flocculation of phytoplankton cells and thus their sinking rates (Avnimelech et al., 1982). SEM images of settling materials give direct evidence of interaction between minerals and organic aggregates (Fig. 4d, e, and f). It is seen clearly that diatom cells are readily inlaid in clay minerals, forming an aggregate (Hamm, 2002). Another evidence for the ballast effect of lithogenic materials is the suspended particle size in the water column (Fig. S2). Suspended particles in HFH have the smallest sizes whose distribution is nearly normal. In contrast, the volume of particle diameter has three peaks in PDR, with the highest peak at the size of ~200 μm, reflecting the flocculation of organic matters. Owing to the combined effect of cyanobacteria-dominated community structure and limited lithogenic minerals input (Fig. 4c and f), organic matter generated via aqueous primary production (autochthonous OM) in HFH is less likely to sink (Avnimelech et al., 1982; Honda and Watanabe, 2010), resulting in a large proportion of the autochthonous OM degraded in the water column. Such speculation is supported by the vertical variation in EC and DO in HFH (Fig. 2). Strong degradation of OM in the hypolimnion during the stratification period consumes almost all dissolved oxygen and causes the EC there much higher than that during the mixing period. This mechanism explains why HFH exhibits high POC concentration, eutrophication level, and primary productivity but low $F_{OC\text{-}auto}$ (Figs. 3a and 8a).

4.3. Carbon sink associated with OC_{auto} burial in the studied reservoirs

Based on the mass within sediment traps in four seasons, we determined the settling flux of OC to be 157 g C/m^2/yr, 359 g C/m^2/yr, and 79 g C/m^2/yr for PZR, PDR, and HFH, respectively. The fractions of OC_{auto} in settling OC are 35.7% at PZR, 33.1% at PDR, and 59.5% at HFH, respectively. Thus, the settling fluxes of OC_{auto} are 56 g C/m^2/yr at PZR, 119 g C/m^2/yr at PDR, and 47 g C/m^2/yr at HFH, respectively (Table 2). It is known that a certain proportion of the settled OC will be remineralized and emitted as CO_2 or CH_4 post sedimentation (Sobek et al., 2009; Ferland et al., 2014; Mendonça et al., 2016; Radbourne et al., 2017). And the degradation rates are different between autochthonous and allochthonous OC, with the former more labile. For example, Sobek et al. (2009) found that the sediments receiving significant input of land-derived OC have the burial efficiency (the ratio of buried OC to settling OC) of 66% while the burial efficiency of the sediments mainly consisting of phytoplankton-derived OC is only 22%. Besides the OC source, the oxygen exposure time is another factor governing the burial efficiency (Sobek et al., 2009; Ferland et al.,

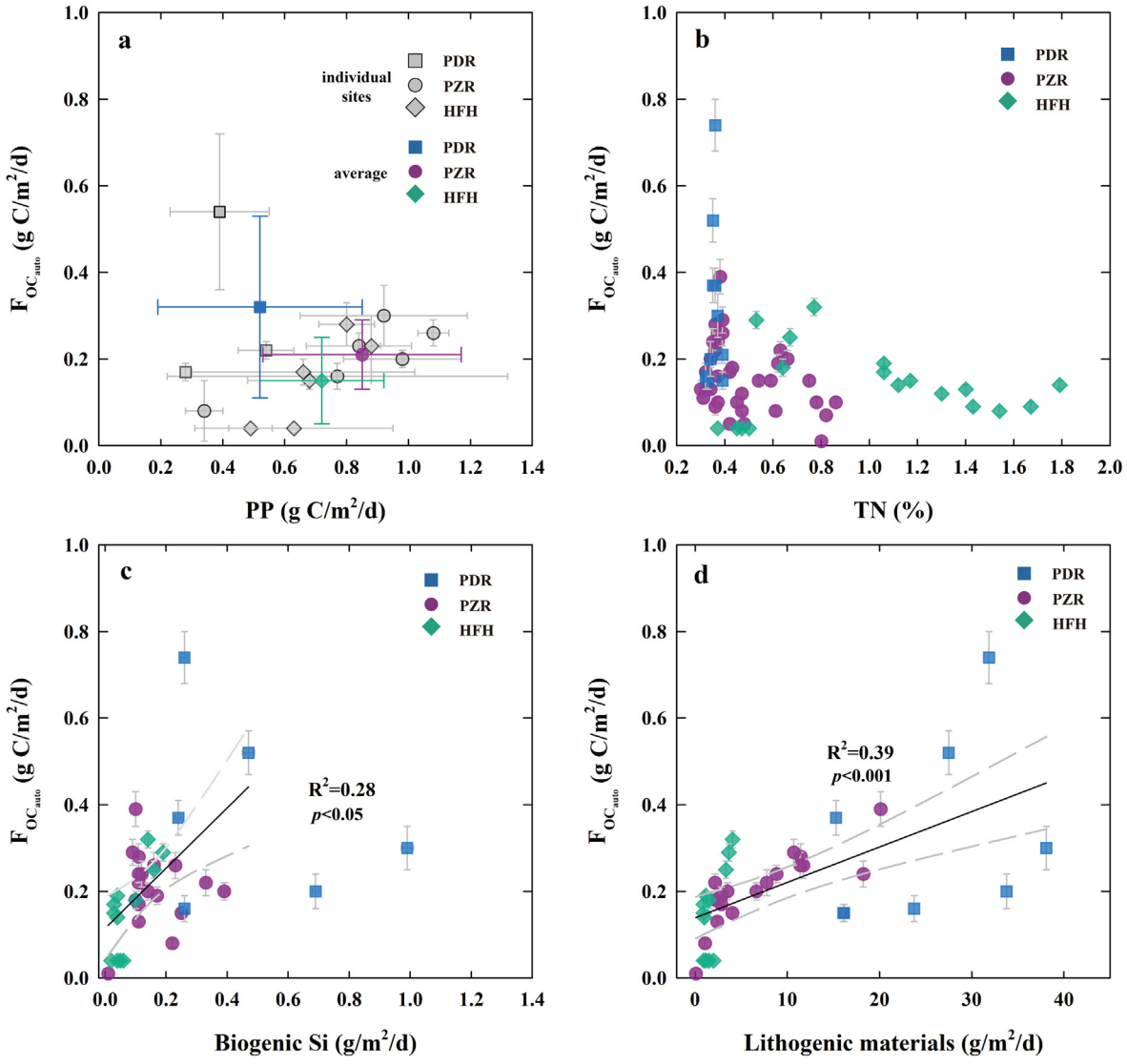

Fig. 8. Scatter plots of primary productivity (PP) versus F_{OC} (a), total nitrogen concentrations (TN) versus F_{OC} (b), biogenic silica fluxes versus F_{OC} (c), and lithogenic materials' fluxes versus F_{OC} in settling particles (d). The circles, rectangles and diamonds represent the Pingzhai Reservoir, Puding Reservoir and Hongfenghu Reservoir, respectively.

2014). More input of lithogenic minerals in the reservoirs with fast flow regime will not only accelerate the sinking of autochthonous OC as suggested in this study but also reduce the oxygen exposure time for settling OC. Results from Mendonça et al. (2016) also show that OC burial efficiency is higher in hydroelectric reservoirs than in natural lakes. If the burial efficiency of OC_{auto} from Sobek et al. (2009)'s study is taken, there is 10– 26 g C/m^2 autochthonous OC would be buried in the three reservoirs annually. Note that this amount of autochthonous OC burial represents an additional carbon sink after damming.

5. Conclusions

To investigate the settling flux of autochthonous OC in reservoirs, we conducted a sediment trap study in three subtropical karst reservoirs SW China. The results show that autochthonous OC accounts for 30– 60% of the total OC in settling particles. And the fraction of autochthonous OC decreases with increasing OC settling flux because of increasing input of allochthonous OC. The flux of autochthonous OC in the three reservoirs varies from 47– 119 g C/m^2/yr. We find that the input of lithogenic

Table 2
Settling flux of autochthonous and allochthonous organic carbon (OC_{auto} and OC_{allo}) in three reservoirs.

	Settling flux of OC_{auto} (g C/m^2/d)			Settling flux of OC_{allo} (g C/m^2/d)		
	Pingzhai Reservoir	Puding Reservoir	Hongfenghu Reservoir	Pingzhai Reservoir	Puding Reservoir	Hongfenghu Reservoir
Spring	0.17	0.19	0.10	0.39	1.33	0.11
Summer	0.24	0.54	0.20	0.35	0.67	0.11
Autumn	0.11	0.29	0.11	0.18	0.33	0.06
Winter	0.11	0.29[a]	0.11	0.20	0.33[a]	0.07
Annual settling flux (g C/m^2/yr)	56	119	47	101	240	32

[a] The flux in Puding Reservoir in autumn is assumed to be the same as that in winter.

minerals and phytoplankton community structure, rather than the primary productivity or trophic state, govern the settling flux of autochthonous OC, which is similar to the ballast effect found in marine environments. To the best of our knowledge, this study is the first time to verify the ballast effect in inland waters. Since inland water receives much more lithogenic materials than the ocean, we suggest that this effect must be considered in the carbon cycle of inland water bodies. In addition, as more hydroelectric reservoirs with short water residence time and fast flow are being built (Maavara et al., 2020) and the changes in land use enhance soil erosion, the role of the ballast effect on the settling of autochthonous OC in inland waters should be more emphasized in the future.

Supplementary data to this article can be found online at https://doi.org/10.1016/j.scitotenv.2021.151736.

CRediT authorship contribution statement

Yu Wei: Investigation, Methodology, Writing - original draft. **Hao Yan:** Conceptualization, Writing - original draft. Supervision, Funding acquisition. **Zaihua Liu:** Writing - review & editing, Supervision, Funding acquisition. **Cuihong Han:** Investigation. **Song Ma:** Investigation. **Hailong Sun:** Investigation. **Qian Bao:** Investigation.

Declaration of competing interest

The authors declare that they have no known competing financial interests or personal relationships that could have appeared to influence the work reported in this paper.

Acknowledgments

We thank Rui Li, Wen Yu, Taiping Ye for their assistances with SEM observation and XRD analysis. We also thank Xiao Tan for the linguistic assistance. Discussion with Huiming Bao and Yongbo Peng are also greatly appreciated. This study was supported by the National Natural Science Foundation of China, China (Grant Nos. U1612441, 41673019, and 41921004), and the Strategic Priority Research Program of Chinese Academy of Sciences, China (Grant No. XDB 40000000). We declare that we have no competing financial interests or personal relationships that could have appeared to influence the work reported in this paper.

References

Armstrong, R.A., Lee, C., Hedges, J.I., Honjo, S., Stuart, W.G., 2001. A new mechanistic model for organic carbon fluxes in the ocean based on the quantitative association of POC with ballast minerals. Deep-Sea Res. PT. II 49 (1-3), 219–236.

Avnimelech, Y., Troeger, B.W., Reed, L.W., 1982. Mutual flocculation of algae and clay: evidence and implications. Science 216 (4541), 63–65.

Barth, J.A., Mader, M., Nenning, F., Van Geldern, R., Friese, K., 2017. Stable isotope mass balances versus concentration differences of dissolved inorganic carbon–implications for tracing carbon turnover in reservoirs. Isot. Environ. Health Stud. 53 (4), 413–426.

Beerling, D., Woodward, F.I., 2001. Vegetation and the terrestrial carbon cycle: the first 400 million years. Ann. Am. Assoc. Geogr. 92 (1), 87–102.

Blattmann, T.M., Liu, Z., Zhang, Y., Zhao, Y., Haghipour, N., Montlucon, D.B., Plotze, M., Eglinton, T.I., 2019. Mineralogical control on the fate of continentally derived organic matter in the ocean. Science 366, 742–745.

Cai, Y., Wan, J., Wang, Y., Wang, B., Wang, R., Wang, J., Wang, L., Wang, Y., Tian, L., Lv, M., Hou, L., Xu, Y., Yan, X., Yang, Z., Yang, S., Wu, D., Wu, X., Zhang, H., Chen, R., Zhou, M., Zhao, Z., Zhao, X., Gao, J., Huang, Q., Peng, J., Lu, Y., 2015. Study on Land Change in Guizhou Karst Plateau Mountain Area. Science Press, Beijing, pp. 61–62 (in Chinese).

Caves Rugenstein, J.K., Ibarra, D.E., von Blanckenburg, F., 2019. Neogene cooling driven by land surface reactivity rather than increased weathering fluxes. Nature 571, 99–102.

Cole, J.J., Prairie, Y.T., Caraco, N.F., Mcdowell, W.H., Tranvik, L.J., Striegl, R.G., Duarte, C.M., Kortelainen, P., Downing, J.A., Middelburg, J.J., Melack, J., 2007. Plumbing the global carbon cycle: integrating inland waters into the terrestrial carbon budget. Ecosystems 10 (1), 172–185.

Cotrufo, M.F., Ranalli, M.G., Haddix, M.L., Six, J., Lugato, E., 2019. Soil carbon storage informed by particulate and mineral-associated organic matter. Nat. Geosci. 12, 989–994.

Dean, W.E., Gorham, E., 1998. Magnitude and significance of carbon burial in lakes, reservoirs, and peatlands. Geology 26 (6), 535–538.

Ferland, M.E., Prairie, Y.T., Teodoru, C., del Giorgio, P.A., 2014. Linking organic carbon sedimentation, burial efficiency, and long-term accumulation in boreal lakes. J. Geophys. Res. Biogeosci. 119 (5), 836–847.

Galy, V., France-Lanord, C., Beyssac, O., Faure, P., Kudrass, H., Palhol, F., 2007. Efficient organic carbon burial in the Bengal fan sustained by the himalayan erosional system. Nature 450, 407–410.

Gardner, W.D., Hinga, K.R., Marra, J., 1983. Observations on the degradation of biogenic material in the deep ocean with implications on accuracy of sediment trap fluxes. J. Mar. Res. 41 (2), 195–214.

Goto, N., Hisamatsu, K., Yoshimizu, C., Ban, S., 2016. Effectiveness of preservatives and poisons on sediment trap material in freshwater environments. Limnology 17 (1), 87–94.

Gu, B., Chapman, A.D., Schelske, C.L., 2006. Factors controlling seasonal variations in stable isotope composition of particulate organic matter in a softwater eutrophic lake. Limnol. Oceamogr. 51 (6), 2837–2848.

Hage, S., Galy, V.V., Cartigny, M.J.B., Acikalin, S., Clare, M.A., Gröcke, D.R., Hilton, R.G., Hunt, J.E., Lintern, D.G., McGhee, C.A., Parsons, D.R., Stacey, C.D., Sumner, E.J., Talling, P.J., 2020. Efficient preservation of young terrestrial organic carbon in sandy turbidity-current deposits. Geology 48, 882–887.

Hamm, C.E., 2002. Interactive aggregation and sedimentation of diatoms and clay-sized lithogenic material. Limnol. Oceamogr. 47 (6), 1790–1795.

Han, C., Sun, H., Wei, Y., Bao, Q., Yan, H., 2020. The temporal and spatial variations of hydrochemistry in karst damped rivers and the carbon fertilization effect of biological carbon pump: a case study of Pingzhai Reservoir and Hongfeng Lake in Guizhou Province. J. Lake Sci. 32 (6), 1683–1694 (In Chinese).

Heathcote, A., Anderson, N.J., Prairie, Y.T., Engstrom, D.R., Giorgio, P.A.D., 2015. Large increases in carbon burial in northern lakes during the Anthropocene. Nat. Commun. 6, 10016.

Honda, M.C., Watanabe, S., 2010. Importance of biogenic opal as ballast of particulate organic carbon (POC) transport and existence of mineral ballast-associated and residual POC in the Western Pacific Subarctic Gyre. Geophys. Res. Lett. 37 (2), 489–496.

Huang, C., Zhang, L., Li, Y., Lin, C., Huang, T., Zhang, M., Zhu, A., Yang, H., Wang, X., 2018. Carbon and nitrogen burial in a plateau lake during eutrophication and phytoplankton blooms. Sci. Total Environ. 616, 296–304.

Huang, S., Pu, J., Li, J., Zhang, T., Cao, J., Pan, M., 2020. Sources, variations, and flux of settling particulate organic matter in a subtropical karst reservoir in Southwest China. J. Hydrol. 586, 124882.

Jiang, Y., Ji, H., 2013. Isotopic indicators of source and fate of particulate organic carbon in a karstic watershed on the Yunnan-Guizhou Plateau. Appl. Geochem. 36, 153–167.

Kennedy, M.J., Pevear, D.R., Hill, R.J., 2002. Mineral surface control of organic carbon in black shale. Science 295, 657–660.

Klaas, C., Archer, D.E., 2002. Association of settling organic matter with various types of mineral ballast in the deep sea: implications for the rain ratio. Glob. Biogeochem. Cycles 16 (4), 1116.

Kunz, M.J., Wüest, A., Wehrli, B., Landert, J., Senn, D.B., 2011. Impact of a large tropical reservoir on riverine transport of sediment, carbon, and nutrients to downstream wetlands. Water Resour. Res. 47 (12), W12531.

Lehner, B., Liermann, C.R., Revenga, C., Vörösmarty, C., Fekete, B., Crouzet, P., Döll, P., Endejan, M., Frenken, K., Magome, J., Nilsson, C., Robertson, J.C., Rödel, R., Sindorf, N., Wisser, D., 2011. High-resolution mapping of the world's reservoirs and dams for sustainable river-flow management. Front. Ecol. Environ. 9 (9), 494–502.

Li, Y.J., Zhang, H.T., Xiao, J., 2019. Effects of river hydrology on phytoplankton dynamics in dammed rivers. Earth Environ. 47 (06), 102–108 (in Chinese).

Liu, T., 2009. Soil Organic Carbon Character and Carbon Isotope Composition of Typical Slope Lands in Karst Areas in Southwest China. Institute of Geochemistry, Chinese Academy of Sciences dissertation thesis.

Liu, Z., Dreybrodt, W., 2015. Significance of the carbon sink produced by H2O–carbonate–CO2–aquatic phototroph interaction on land. Sci. Bull. 60 (2), 182–191.

Liu, Z., Zhao, M., Sun, H., Yang, R., Chen, B., Yang, M., Zeng, Q., Zeng, H., 2017. "Old" carbon entering the South China Sea from the carbonate-rich Pearl River Basin: coupled action of carbonate weathering and aquatic photosynthesis. Appl. Geochem. 78, 96–104.

Liu, Z., Macpherson, G.L., Groves, C., Martin, J.B., Yuan, D.X., Zeng, S., 2018. Large and active CO2 uptake by coupled carbonate weathering. Earth-Sci. Rev. 182, 42–49.

Maavara, T., Parsons, C.T., Ridenour, C., Stojanovic, S., Dürr, H.H., Powley, H.R., Van Cappellen, P., 2015. Global phosphorus retention by river damming. Proc. Natl. Acad. Sci. U. S. A. 112 (51), 15603–15608.

Maavara, T., Lauerwald, R., Regnier, P., 2017. Global perturbation of organic carbon cycling by river damming. Nat. Commun. 8, 15347.

Maavara, T., Chen, Q., Van Meter, K., Brown, L.E., Zarfl, C., 2020. River dam impacts on biogeochemical cycling. Nat. Rev. Earth Environ. 1, 103–116.

Maki, K., Kim, C., Yoshimizu, C., Tayasu, I., Miyajima, T., Nagata, T., 2010. Autochthonous origin of semi-labile dissolved organic carbon in a large monomictic lake (Lake Biwa): carbon stable isotopic evidence. Limnology 11 (2), 143–153.

Marwick, T.R., Tamooh, F., Teodoru, C.R., Borges, A.V., Darchambeau, F., Bouillon, S., 2015. The age of river-transported carbon: a global perspective. Glob. Biogeochem. Cycles 29 (2), 122–137.

Mendonça, R., Kosten, S., Sobek, S., Barros, N., Cole, J.J., Tranvik, L., Roland, F., 2012. Hydroelectric carbon sequestration. Nat. Geosci. 5 (12), 838–840.

Mendonça, R., Kosten, S., Sobek, S., Cole, J., Bastos, A., Albuquerque, A., Cardoso, S., Roland, F., 2014. Carbon sequestration in a large hydroelectric reservoir: an integrative seismic approach. Ecosystems 17, 430–441.

Mendonça, R., Kosten, S., Sobek, S., Cardoso, S.J., Figueiredo-Barros, M.P., Estrada, C.H.D., Roland, F., 2016. Organic carbon burial efficiency in a subtropical hydroelectric reservoir. Biogeosciences 13 (11), 3331–3342.

Mendonça, R., Muller, R.A., Clow, D., Verpoorter, C., Sobek, S., 2017. Organic carbon burial in global lakes and reservoirs. Nat. Commun. 8 (1), 1694.

Meyers, P.A., 1994. Preservation of elemental and isotopic source identification of sedimentary organic matter. Chem. Geol. 114 (3–4), 289–302.

Meyers, P.A., Ishiwatari, R., 1993. Lacustrine organic geochemistry—an overview of indicators of organic matter sources and diagenesis in lake sediments. Org. Geochem. 20 (7), 867–900.

Mulholland, P.J., Elwood, J.W., 1982. The role of lake and reservoir sediments as sinks in the perturbed global carbon cycle. Tellus 34 (5), 490–499.
Passow, U., De La Rocha, C.L., 2006. Accumulation of mineral ballast on organic aggregates. Glob.Biogeochem. Cycles 20, GB1013.
Perdue, E.M., Koprivnjak, J.F., 2007. Using the C/N ratio to estimate terrigenous inputs of organic matter to aquatic environments. Estuar. Coast. Shelf Sci. 73 (1–2), 65–72.
Pu, J., Li, J., Zhang, T., Martin, J.B., Yuan, D., 2020. Varying thermal structure controls the dynamics of CO2 emissions from a subtropical reservoir, south China. Water Res. 178, 115831.
Radbourne, A.D., Ryves, D.B., Anderson, N.J., Scott, D.R., 2017. The historical dependency of organic carbon burial efficiency. Limnol. Oceamogr. 62 (4), 1480–1497.
Raymond, P.A., 2005. Carbon cycle: the age of the Amazon's breath. Nature 436 (7050), 469.
Raymond, P.A., Hartmann, J., Lauerwald, R., Guth, P., 2013. Global carbon dioxide emissions from inland waters. Nature 503 (7476), 355–359.
Rixen, T., Gaye, B., Emeis, K.C., 2019. The monsoon, carbon fluxes, and the organic carbon pump in the northern Indian Ocean. Prog. Oceanogr. 175, 24–39.
Rodríguez-Murillo, J.C., Filella, M., 2015. Temporal evolution of organic carbon concentrations in Swiss lakes: trends of allochthonous and autochthonous organic carbon. Sci. Total Environ. 520, 13–22.
Schimel, D., Stephens, B.B., Fisher, J.B., 2015. Effect of increasing CO2 on the terrestrial carbon cycle. Proc. Natl. Acad. Sci. U. S. A. 112 (2), 436.
Shi, J., Wang, B., Wang, F., Peng, X., 2018. Sources and fluxes of particulate organic carbon in the Wujiang cascade reservoirs, Southwest China. Inland Waters 8 (2), 141–147.
Sitch, S., Huntingford, C., Gedney, N., Levy, P.E., Lomas, M., Piao, S.L., Betts, R., Ciais, P., Cox, P., Friedlingstein, P., Jones, C.D., Prentice, I.C., Woodward, F.I., 2008. Evaluation of the terrestrial carbon cycle, future plant geography and climate-carbon cycle feedbacks using five dynamic global vegetation models (DGVMs). Glob. Chang. Biol. 14 (9), 2015–2039.
Smith, T.M., Cramer, W.P., Dixon, R.K., Leemans, R., Neilson, R.P., Solomon, A.M., 1993. The global terrestrial carbon cycle. Water Air Soil Pollut. 70 (1–4), 19–37.
Sobek, S., Durisch-Kaiser, E., Zurbrügg, R., Wongfun, N., Wessels, M., Pasche, N., Wehrli, B., 2009. Organic carbon burial efficiency in lake sediments controlled by oxygen exposure time and sediment source. Limnol. Oceanogr. 54 (6), 2243–2254.
Tao, F.X., Liu, C.Q., Li, S.L., 2009. Source and flux of POC in two subtropical karstic tributaries with contrasting land use practice in the Yangtze River Basin. Appl. Geochem. 24 (11), 2102–2112.
Tao, S., Eglinton, T.I., Montluçon, D.B., McIntyre, C., Zhao, M., 2015. Pre-aged soil organic carbon as a major component of the Yellow River suspended load: regional significance and global relevance. Earth Planet. Sci. Lett. 414, 77–86.
Tranvik, L.J., Downing, J.A., Cotner, J.B., Loiselle, S.A., Striegl, R.G., Ballatore, T.J., Dillon, P., Finlay, K., Fortino, K., Knoll, L.B., 2009. Lakes and reservoirs as regulators of carbon cycling and climate. Limnol. Oceanogr. 54 (6), 2298–2314.
Tranvik, L.J., Cole, J.J., Prairie, Y.T., 2018. The study of carbon in inland waters—from isolated ecosystems to players in the global carbon cycle. Limnol. Oceanogr. Lett. 3 (3), 41–48.
Wang, S.F., Zhang, Y.L., Li, J., 2011. Study on the chlorophyll-a and primary production in the Luanhe-Beidaihe Estuary. Key Eng. Mater. 474–476, 1288–1291.
Wang, B., Liu, C.-Q., Peng, X., et al., 2013. Mechanisms controlling the carbon stable isotope composition of phytoplankton in karst reservoirs. J. Limnol. 72 (1), e11.
Wang, H., Gao, J., Hou, W., 2019. Quantitative attribution analysis of soil erosion in different geomorphological types in karst areas: based on the geodetector method. J. Geogr. Sci. 29 (2), 271–286.
Wei, Y., Yang, C., Yan, H., Liu, Z., 2020. Coupled cycling of carbon and silica in Karst Reservoirs: insights from Hongfeng Lake, Puding Reservoir and Pingzhai Reservoir. Earth Environ. 48 (01), 1–9 (In Chinese).
Xiang, P., Wang, S.L., Yang, Y., Huang, Q., 2016. Distribution and retention efficiency of nitrogen and phosphorous in cascade reservoirs in Wujiang River basin. Earth Environ. 44 (05), 492–501 (In Chinese).
Xiao, J., Wang, B., Zhang, H., Shi, J., Qiu, X., Liu, T., 2019. Succession of phytoplankton functional groups in the Wujiang river-reservoir system and its environment impact factors identification. Earth Environ. 47 (06), 829–838 (In Chinese).
Yang, M., Liu, Z., Sun, H., Yang, R., Chen, B., 2016. Organic carbon source tracing and DIC fertilization effect in the pearl river: insights from lipid biomarker and geochemical analysis. Appl. Geochem. 73, 132–141.
Yang, Y., Peng, X., Lu, W., Wang, S., 2017. The sedimentation rate and burial fluxes of carbon and nitrogen in wujiangdu reservoir, Guizhou,China. Earth Environ. 45 (1), 66–73 (In Chinese).
Yu, Q., Wang, F., Yan, W., Zhang, F., Lv, S., Li, Y., 2018. Carbon and nitrogen burial and response to climate change and anthropogenic disturbance in Chaohu Lake, China. Int. J. Env. Res. Public Health 15 (12), 2734.
Zeng, S., Kaufmann, G., Liu, Z., 2019. Sensitivity of the global carbonate weathering carbon-sink flux to climate and land-use changes. Nat. Commun. 10, 5749.
Zheng, L.-W., Li, D., Ding, X., Lee, T.-Y., Zheng, Z., Shiah, F.-K., Zheng, X., Hsu, T.-C., Huang, J.-C., Kao, S.-J., 2020. Isotope constraints on the sources of particulate organic carbon in a subtropical deep reservoir. J. Geophys. Res.-Biogeosci. 125 (1), e2019JG005240.